Quantumclassical reaction path study of the reaction O(3 P)+O3(1 A 1)→2O2(X 3Σ− g)

N. Balakrishnan and G. D. Billing

Citation: The Journal of Chemical Physics **104**, 9482 (1996); doi: 10.1063/1.471691
View online: http://dx.doi.org/10.1063/1.471691
View Table of Contents: http://scitation.aip.org/content/aip/journal/jcp/104/23?ver=pdfcov
Published by the AIP Publishing

Quantum-classical reaction path study of the reaction $O(^3P)+O_3(^1A_1)\rightarrow 2O_2(X\ ^3\Sigma_g^-)$

N. Balakrishnan and G. D. Billing
Chemistry Laboratory III, H. C. Ørsted Institute, University of Copenhagen, DK 2100 Copenhagen, Denmark

(Received 16 January 1996; accepted 13 March 1996)

The atmospheric reaction $O(^3P)+O_3(^1A_1)\rightarrow 2O_2(X\ ^3\Sigma_g^-)$ is studied using the reaction path approach. In addition to total reaction rate constants and cross sections, product vibrational state-resolved cross sections and rate constants are computed. The product vibrational state distribution shows that one of the product O_2 molecules is formed in a higher vibrational state than the other with a broad distribution the tail of which extends beyond $v=27$. However, no bimodal pattern is seen in the vibrational distribution in contrast to that found for O_2 molecules resulting from O_3 photodissociation in recent experimental studies. The vibrational excitation of the product O_2 molecules is found to be mainly due to the large increase in the coupling element which couples the reaction path motion to the perpendicular vibrational motion. © *1996 American Institute of Physics.* [S0021-9606(96)01523-1]

I. INTRODUCTION

The reaction

$$O(^3P)+O_3(^1A_1)\rightarrow 2O_2(X\ ^3\Sigma_g^-) \qquad (R_1)$$

is one of the most important reactions in stratospheric chemistry and plays a crucial role in the global abundance of ozone concentration. Numerous kinetic studies have been performed on it over the years and extensive compilations of its rate constants have become available at temperatures of atmospheric interest.[1–7] This reaction has received much attention in recent years partly because of the activity in four-atom reactive systems and more importantly due to the involvement of highly vibrationally excited O_2 molecules in addressing[8–12] the ''ozone deficit'' problem. Recently, it has been observed that photolysis of ozone below 248 nm produces highly vibrationally excited O_2 molecules[10–13] and Slanger *et al.*[8] have proposed an autocatalytic mechanism for O_3 production involving vibrationally excited O_2 molecules. Furthermore, recent time-resolved experiments of Wodtke and co-workers[12] have observed a bimodal translational energy distribution of the recoiling O atom from O_3 photodissociation. From this they deduced a similar bimodal vibrational distribution for the O_2 product with one peak around $v=14$ and another near $v=27$. A similar study by Sayage[14] also recently confirmed the bimodal vibrational distribution of the O_2 fragment. These highly vibrationally excited O_2 molecules posses enough energy for the reverse of reaction (R_1) to be energetically feasible. Based on this Wodtke and co-workers[10–12] have proposed a new mechanism for O_3 production in which a highly vibrationally excited O_2 molecule collides with a ground vibrational state O_2 to produce O_3 and hence account partly for the discrepancy between measured and modeled ozone concentration at altitudes of about 50 kms from earth's surface. The above proposition is yet to be verified as direct detection of ozone produced from the bimolecular reaction was not done in the experiment. However, in a recent re-evaluation of the ozone budget problem, Crutzen *et al.*[15] argued that the discrepancy vanishes under new modeling conditions with out the inclusion of the newly proposed source of ozone. Nevertheless, considering the importance of the suggested mechanism, the above proposition has created renewed experimental and theoretical interest in ozone chemistry and in particular on reaction (R_1) and its reverse process

$$O_2(v'\gg 1)+O_2(v''=0)\rightarrow O_3+O. \qquad (R_2)$$

This process is highly endothermic and requires an activation energy of over 4 eV if the two molecules are in the ground vibrational state but becomes energetically feasible for $v'\geqslant 27$. If this does happen, then on similar accounts it is naturally expected that the exothermicity of reaction (R_1) goes mostly into O_2 internal energy. Thus investigation of the vibrational distribution of the O_2 products resulting from reaction (R_1) is important in complementing the proposed mechanism for O_3 production via (R_2). As part of the recent developments in four-atom reaction dynamics, some attention has been given to reaction (R_1)[16,17] but mainly from the point of view of thermal rate constants. Recently, we have computed rate constants for reaction (R_1)[18] using variational transition state theory (VTST) which gave results in satisfactory agreement with experimental results as well as QCT[16] and approximate quantum mechanical calculations.[17] We have also performed[18] some preliminary investigation of reaction (R_2) with $27\leqslant v'\leqslant 30$ using a semiclassical scheme[19–21] which was successfully applied to $OH+H_2$ and $OH+CO$ reactions. Within the limited number of trajectories performed and the accuracy of the potential energy surface (PES) employed, our calculations have not been able to confirm the experimental observation. Though significant advances have been made in four-atom reactive scattering calculations in recent years,[19–30] rigorous state-to-state four-atom reactive scattering calculations are yet to become realizable. The present system, owing to the presence of four heavy O atoms is anyway not going to be amenable to such calculations in the near future. Thus, in the present paper, we

 0021-9606/96/104(23)/9482/13/$10.00

use the reaction path approach of Billing[31–37] to study reaction (R_1). The approach has previously been tested on the H_2+OH reaction. The comparison with other approximate methods as classical trajectory calculations and variational transition state calculations is generally good[34,36] except at higher temperatures, where the reaction path rates are smaller than those obtained by, e.g., transition state calculations. A similar tendency is found for the reaction studied here.

Although the reaction path approach provides only an approximate description of the dynamics, it has the advantage that it can provide final vibrational state resolution of the product molecules which is the main motivation behind the present study. An analysis of the product vibrational distribution from reaction (R_1) can also provide sufficient insight into the feasibility of the proposed mechanism for ozone formation (R_2). To the best of our knowledge, this is the first investigation in which vibrational distribution of the O_2 molecules from reaction (R_1) is investigated.

The paper is organized as follows: Sec. II gives a brief description of the reaction path approach. The results of our calculation are given in Sec. III together with a discussion and a summary of our findings is given in Sec. IV.

II. REACTION PATH APPROACH

Since the reaction path method has been discussed in detail in a number of earlier publications,[31–37] only a brief description is given here. This is a very useful method to treat systems with a large number of degrees of freedom. As the dimensionality of the system increases, it is impossible to obtain a full 3N-6 dimensional PES for the system and perform a full scattering calculation. In reaction path method[31–37] the bulk part of the system which by and large remains as a spectator is treated approximately and the phase space relevant for the reaction (reaction path) is projected out. Thus, the motion of the system is approximated as that of a fictitious particle (with appropriate reduced mass) along the reaction path. In the present study, the translational motion along the reaction path and the overall rotational motion of the complex are treated classically and the vibrations perpendicular to the reaction path are treated quantum mechanically within the harmonic approximation.

Although only limited information about the PES is necessary in reaction path calculations, one can use the full 3N-6 dimensional PES to obtain the reaction path information if it is available. For the present system, we have used the full six-dimensional semi-empirical PES due to Varandas and Pais[16] based on double many-body expansion method (DMBE) to extract reaction path information. The reaction path (s) as well as normal mode frequencies [$w_k(s)$, $k=1$, M, and $M=3N-7$ where N is the number of atoms] along the reaction path for the present system have been reported recently.[18] In order to avoid the difficulties in dealing with a large number of states in the usual state expansion methods, the reaction path Hamiltonian is cast in second quantized form using a Harmonic approximation for the oscillator coordinates. The actual derivation of the reaction path Hamiltonian can be found elsewhere[31,32] and only details pertaining to the present study are given here. The reaction path dynamics is governed by the effective Hamiltonian,[31–37]

$$H_{\rm eff}=\frac{1}{2}\,p_s^2+V(s)+H_{\rm rot}+\sum_k\ \hbar\tilde{\omega}_k\left(\frac{1}{2}+\rho_k(t)\right)+i\sum_k\ (F_k^-P_k^+-F_k^+P_k^-)+\sum_{kl,k>l}\ \{[F_{kl}^+(n_k^0Q_{kl}+n_l^0Q_{lk}^*+\alpha_l^+\alpha_k^-)]+[F_{kl}^-(n_k^0Q_{kl}^*+n_l^0Q_{lk}+\alpha_l^-\alpha_k^+)]\}. \tag{1}$$

The first term in Eq. (1) is the kinetic energy for relative motion along s. $V(s)$ is the potential as a function of s and $H_{\rm rot}$ is the Hamiltonian for the rotational motion which is defined as

$$H_{\rm rot}=\frac{1}{2}\sum_\alpha\ P_\alpha^2/I_{\alpha\alpha}^e(s);\quad(\alpha=x,y,z), \tag{2}$$

where $I_{\alpha\alpha}^e$ are the principal axes moments of inertia of the complex along the reaction path and the momenta P_x, P_y, and P_z may be expressed in terms of Euler angles describing the overall rotation of the complex and their conjugate momenta. The fourth term in Eq. (1) represents the internal energy of the molecular system in the perpendicular vibrational modes including the zero point vibrational energy. The modulated vibrational frequency $\tilde{\omega}_k$ is defined as

$$\tilde{\omega}(s)=\omega_k(s)+\tfrac{1}{2}p_s^2\tilde{C}_{kk}(s)/\omega_k(s), \tag{3}$$

where the frequency modulation terms $\tilde{C}_{kk}$ will be defined below. The parameter ρ_k is a measure of the excitation of each mode and is given by

$$\rho_k=n_k^0+\sum_j\ n_j^0Q_{jk}Q_{jk}^*+P_k^+P_k^-\,, \tag{4}$$

where n_k^0 are the initial normal mode vibrational quantum numbers and P_k^+ is defined as

$$P_k^+=\alpha_k^++\sum_{j=1}^{M}\ Q_{jk}\alpha_j^+\,, \tag{5}$$

where

$$\alpha_k^+=-\frac{1}{\hbar}\int dt\left(F_k^++\sum_j^M\ F_j^+Q_{jk}^*\right). \tag{6}$$

P_k and α_k are complex quantities such that $P_k^-=(P_k^+)^*$ and $\alpha_k^-=(\alpha_k^+)^*$. F_k is defined as

$$F_k^\pm=f_k\,\exp(\pm i\,\theta_k), \tag{7}$$

where the phase factor θ_k is defined in terms of the modulated vibrational frequency $\tilde{\omega}_k$ as

$$\theta_k=\int dt\ \tilde{\omega}_k(s(t)). \tag{8}$$

The quantity f_k in Eq. (7) is the generalized force for mode k linear in normal mode coordinates:

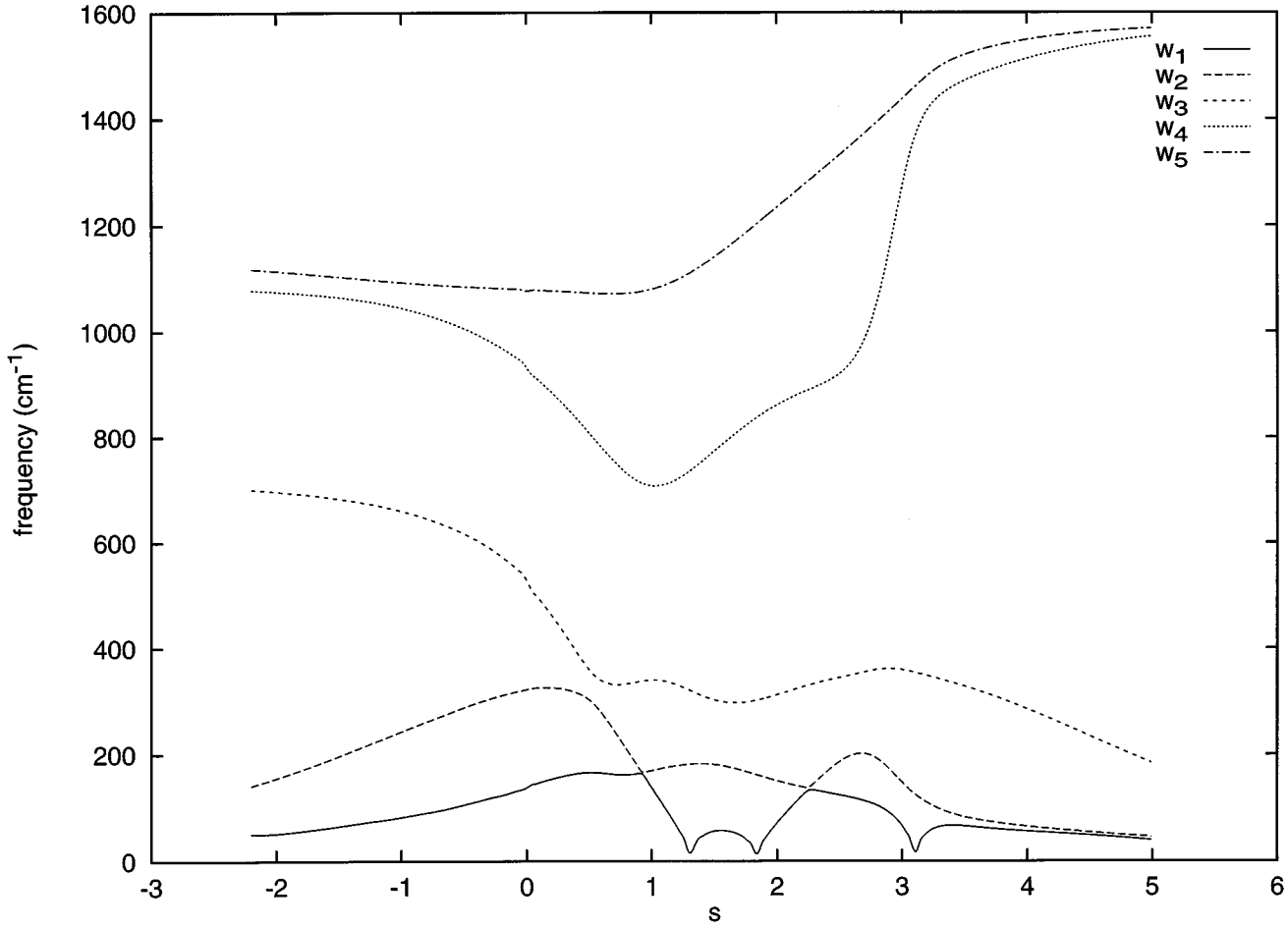

FIG. 1. Frequencies of vibration orthogonal to the reaction path as a function of the reaction path (in units amu$^{1/2}$ Å).

$$f_k=-b_k(s)\left(p_s^2 B_{kF}(s)+\sum_{\alpha\beta}\frac{P_\alpha P_\beta a_k^{\alpha\beta}}{I^e_{\alpha\alpha}I^e_{\beta\beta}}\right), \tag{9}$$

where

$$b_k(s)=\sqrt{\frac{\hbar}{2\omega_k(s)}} \tag{10}$$

and

$$\alpha_k^{\alpha\beta}=\sum_i \sqrt{m_i}[a_{i\beta}l_{ik}^{(\alpha)}+a_{i\alpha}l_{ik}^{(\beta)}]. \tag{11}$$

In the above equation, $\mathbf{l}_{ik}=(l_{ik}^x,l_{ik}^y,l_{ik}^z)$ are the orthogonal displacement vectors connecting the ith particle to the κth normal mode coordinate. Similarly, $\mathbf{a}_i(s)=(a_{ix},a_{iy},a_{iz})$ is the position vector of the atom i along the reaction path. Numerical procedures to compute $\mathbf{l}_{ik}$ and $\mathbf{a}_i(s)$ along the reaction path are discussed in detail in the appendix of Ref. 33. Once $\mathbf{a}_i(s)$ is calculated, the moments of inertia may be evaluated easily as

$$I^e_{\alpha\alpha}=\sum_i m_i(a_{i\beta}^2+a_{i\gamma}^2);\quad(\alpha\neq\beta\neq\gamma). \tag{12}$$

Thus, the fifth term in Eq. (1) arises from the expectation value of the linear term of the intermolecular potential function (which is assumed to be expanded up to second order in the oscillator coordinates) and is referred to as the V–T (vibration–translation) coupling term. The V–T term mainly depends on the linear force, f_k, the first term of which contains p_s^2, the coupling term B_{kF} which couples the reaction path to the perpendicular vibrational mode k, and a matrix element $b_k(s)$ of the second quantized creation and annihilation operators. The second term in f_k is a Coriolis type term which does not induce vibrational transition but tries to distort (stretch or bend) the molecule during the rotation of the complex and is referred to as the ''centrifugal stretch term.'' The last term in $\{\cdots\}$ in Eq. (1) arises from the expectation value of the quadratic term of the potential and is the V–V (vibration-vibration) coupling term. The quadratic forces are given by the expression

$$F_{kl}^+=f_{kl}\exp[i(\theta_k-\theta_l)], \tag{13}$$

where

$$f_{kl}=p_s\left[b_k b_l\left(\frac{1}{2}p_s\widetilde{C}_{kl}+\sum_{k'}B_{k'l}\sum_{\alpha=x,y,z}P_\alpha\zeta_{kk'}^\alpha/I^e_{\alpha\alpha}(s)\right)-i\hbar\omega_+B_{kl}\right], \tag{14}$$

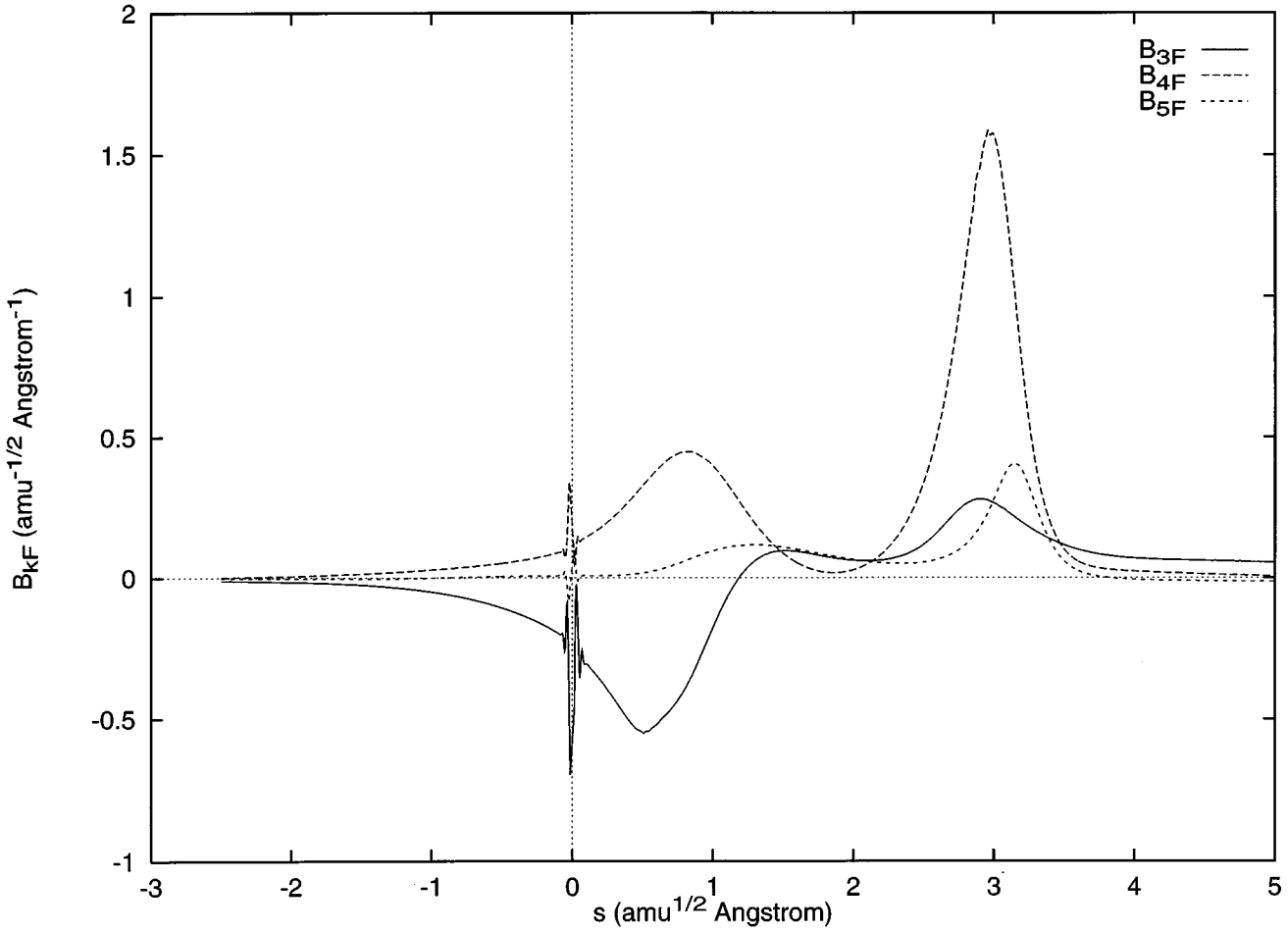

FIG. 2. Coupling elements B_{3F}, B_{4F}, and B_{5F} as a function of the reaction path.

where ω_+ and $\widetilde{C}_{kl}$ are defined as

$$\omega_+=(\omega_k+\omega_l)/\sqrt{\omega_k\omega_l} \tag{15}$$

and

$$\widetilde{C}_{kl}=4B_{kF}B_{lF}-C_{kl}+\sum_{k'} B_{k'k}B_{k'l}. \tag{16}$$

The directions of cosines $\zeta^{\alpha}_{kk'}$ are defined in terms of the orthogonal displacement vectors $\mathbf{l}_{ik}$:

$$\zeta^{\alpha}_{kk'}=\sum_i (l^{\beta}_{ik}l^{\gamma}_{ik'}-l^{\gamma}_{ik}l^{\beta}_{ik'}). \tag{17}$$

The different coupling elements B_{kF}, $B_{kk'}$, and $C_{kk'}$ are defined as follows:

$$B_{kF}=\sum_i \frac{d}{ds}\mathbf{l}_{ik}\cdot\mathbf{l}_{iF}, \tag{18}$$

$$B_{kk'}=\sum_i \frac{d}{ds}\mathbf{l}_{ik}\cdot\mathbf{l}_{ik'}, \tag{19}$$

$$C_{kk'}=\sum_i \frac{d}{ds}\mathbf{l}_{ik}\cdot\frac{d}{ds}\mathbf{l}_{ik'}, \tag{20}$$

where the subscript F indicates reaction path and k denotes the $3N-7$ vibrational degrees of freedom. Numerical procedures to compute the orthogonal displacement vectors $\mathbf{l}_{ik}$ and $\mathbf{l}_{iF}$ are also given in the appendix of Ref. 33. The potential, harmonic vibrational frequencies, position vectors of different atoms and their orthogonal displacement vectors are computed along the reaction path (s) and are spline fitted in a convenient form for use in reaction path dynamics. Once the displacement vectors are known, the coupling elements can be evaluated at the appropriate s values during the dynamics. As mentioned above, the quadratic coupling terms (F_{kl}) are responsible for energy transfer to perpendicular vibrational modes. Thus, in order to obtain the amplitudes of vibrational transitions one has to solve the system of coupled equations[32–37]

$$i\hbar\dot{\mathbf{R}}=\mathbf{AR}, \tag{21}$$

where $\mathbf{R}=\mathbf{Q}+\mathbf{I}$ with $\mathbf{R}(-\infty)=\mathbf{I}$ and $\mathbf{I}$ is a unit matrix. The elements A_{kl} are obtained as $A_{kl}=F^{+}_{kl}$ for $(k>l)$ and $A_{lk}=F^{-}_{kl}=(F^{+}_{kl})^*$ for $(l<k)$. The V–V transition amplitudes are extracted from the $\mathbf{Q}$ matrix by solving the inversion problem discussed in detail in Ref. 32 and 38. The above

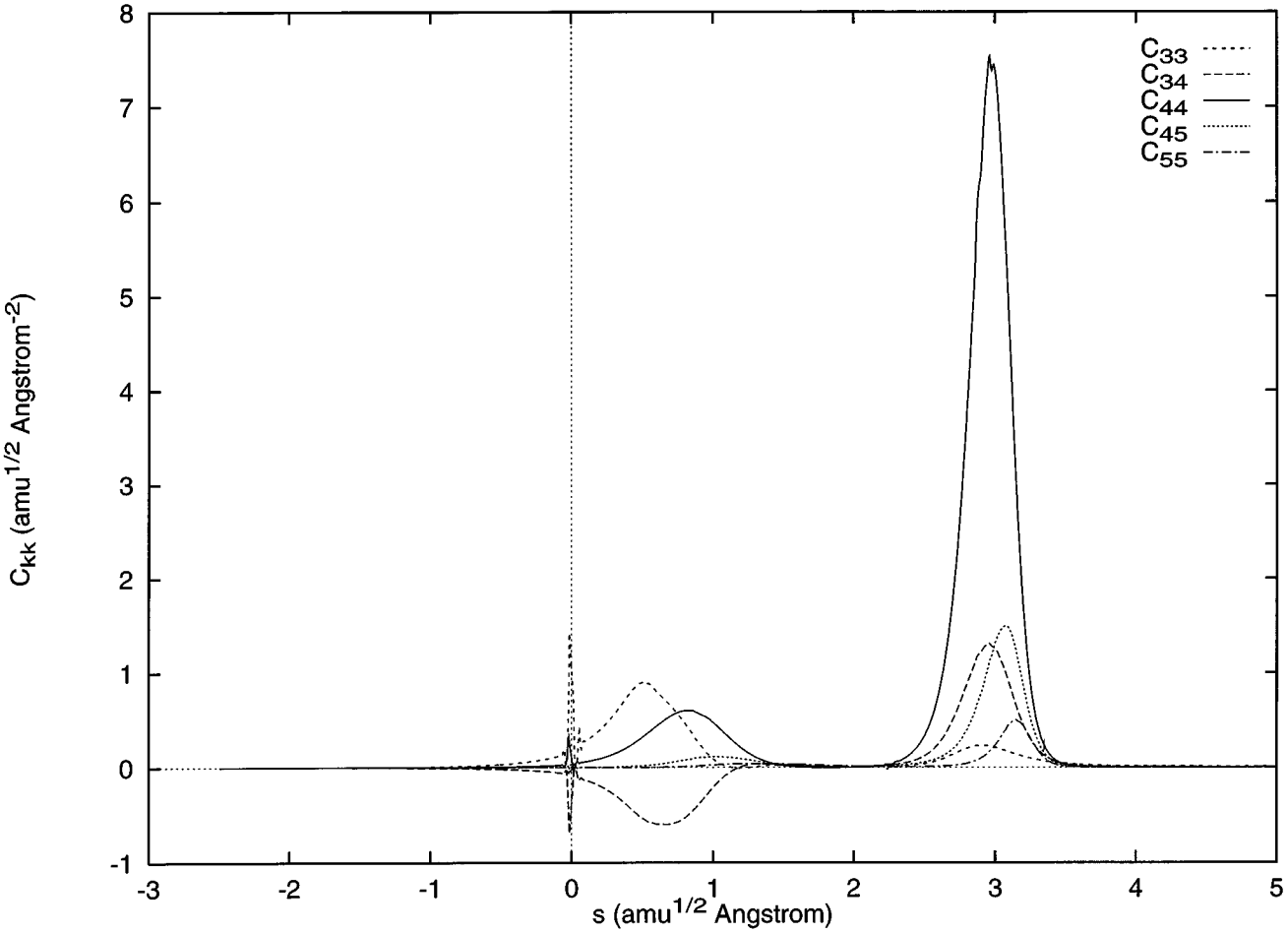

FIG. 3. Coupling elements $\widetilde{C}_{33}$, $\widetilde{C}_{34}$, $\widetilde{C}_{44}$, $\widetilde{C}_{45}$, and $\widetilde{C}_{55}$ as a function of the reaction path.

system of coupled equations together with the equations for θ_k, α_k, and β_k where the phase factor β_k is given by[33,34]

$$\beta_k = 2i \int dt(\alpha_k^+ \dot{\alpha}_k^- - \alpha_k^- \dot{\alpha}_k^+) \tag{22}$$

are integrated along with the equations of motion for the classical variable (s, p_s, and the Euler angles and the corresponding momenta). The amplitude of energy transfer from a set of initial vibrational states $\{n_i\}$ to final vibrational states $\{n_f\}$ is given by

$$\langle\{n_f\}|U|\{n_i\}\rangle = \sum_{\{k\}} \langle\{n_f\}|U_{\mathrm{VV}}|\{k\}\rangle\langle\{k\}|U_{\mathrm{VT}}|\{n_i\}\rangle, \tag{23}$$

where the evolution operator U has been decomposed into a V–T and V–V part with

$$\langle\{k\}|U_{\mathrm{VT}}|\{n_i\}\rangle = \prod_{k=1}^{M} U_{\mathrm{VT}}^{(k)}. \tag{24}$$

The individual V–T amplitudes are given by

$$U_{\mathrm{VT}}^{(k)} = \exp\left(i\beta_k - \frac{1}{2}\rho_k\right)\sqrt{(n_i!n_k!)}(i\alpha_k^+)^{(n_k-n_i)} \times \sum_{p=0}^{n_i} \frac{(-1)^p \rho_k^p}{p!(n_k-n_i+p)!(n_i-p)!}. \tag{25}$$

As mentioned above, the V–V amplitudes are obtained by solving the inversion problem. The solution to this for the general M-quantum case has been given by Billing.[32,38]

A. Initialization of the reaction path dynamics

The reaction path dynamics is initialized at a value of $s=s_0$ where the various coupling terms vanish. A rotational adiabatic assumption[34,35] is made at s_0 where the Hamiltonian $H_{\mathrm{rot}}=H_{\mathrm{rot}}(s_0)$ is set equal to the O_3 rotational energy and the orbital energy:

$$H_{\mathrm{rot}}(s_0) = \frac{\hbar^2 l(l+1)}{2\mu R^2(s_0)} + \frac{\hbar^2}{2I_1}\left[j(j+1)+K^2\left(\frac{I_1}{I_3}-1\right)\right], \tag{26}$$

where $R(s_0)$ is the center-of-mass distance at $s=s_0$, μ the reduced mass for relative motion, and I_k the moments of inertia of the O_3 molecule. The above expression for rotational energy is that for a symmetric top ($I_1=I_2>I_3$) molecule. However, one can use the same expression for slightly asymmetric molecule such as O_3 by introducing[35]

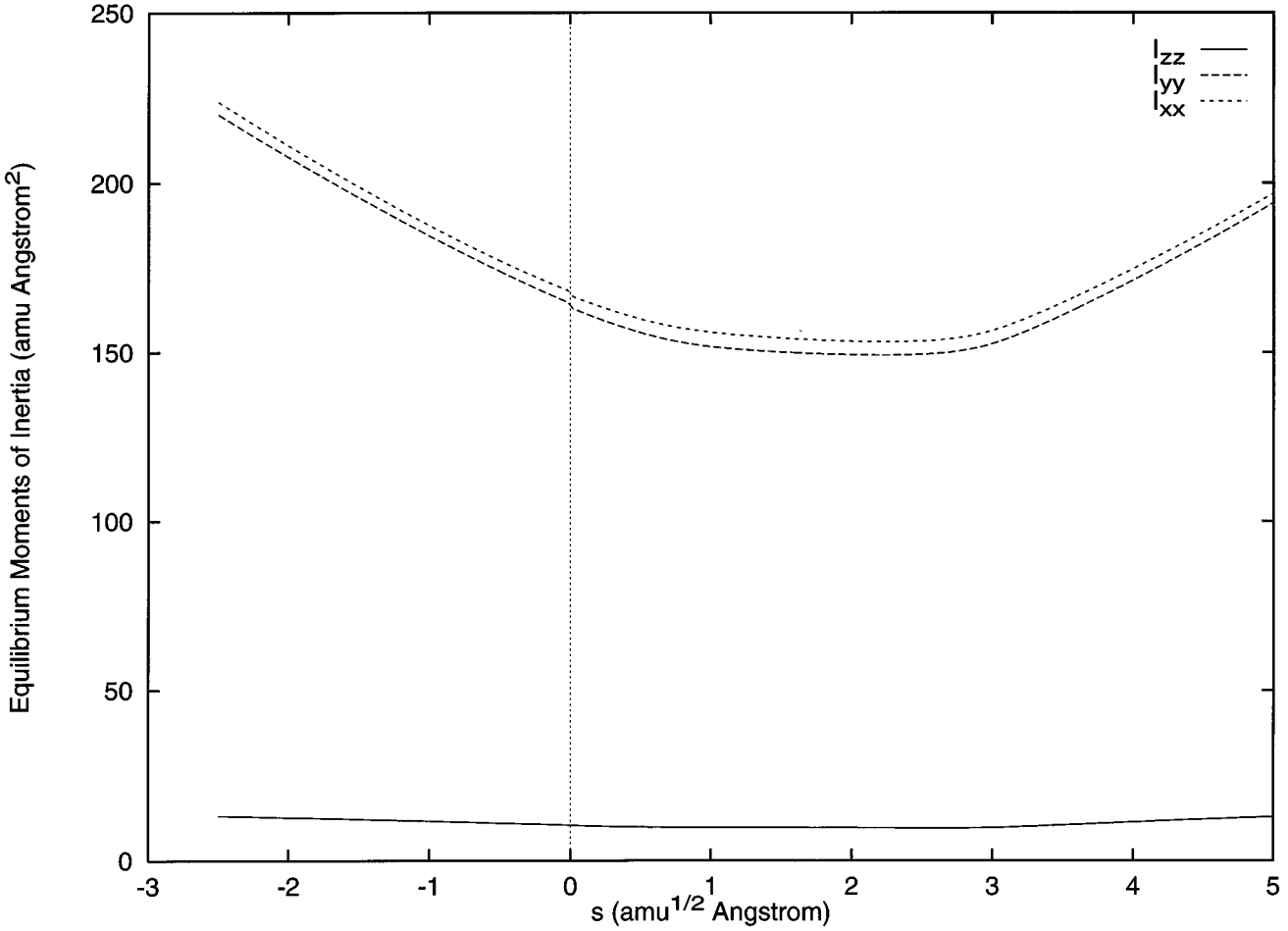

FIG. 4. Principal axes moments of inertia of the complex as a function of the reaction path.

$$I=\sqrt{I_1 I_2} \tag{27}$$

and use it in place of I_1 in Eq. (26). The initial kinetic energy is defined as

$$E_{\rm kin}(s_0)=E_{\rm kin}-\frac{\hbar^2 l(l+1)}{2\mu R^2(s_0)}-V(s_0)-\Delta E_{\rm vib}(s_0) \tag{28}$$

where $\Delta E_{\rm vib}(s_0)$ is the difference in vibrational energy at $s=-\infty$ and s_0:

$$\Delta E_{\rm vib}(s_0)=\hbar\sum_k\ [\omega_k(s_0)(n_k^0+1/2) - \omega_k(-\infty)(n_k^0+1/2)]. \tag{29}$$

Since s_0 is chosen such that the coupling is negligible in the region $[-\infty,s_0]$, the above vibrational adiabatic assumption is not a serious restriction on the dynamics. The equations for the classical degrees of freedom and the coupled equations for energy transfer to the vibrational modes are integrated from s_0 to $s_{\rm max}$ where $s_{\rm max}$ is chosen to be large enough in the product channel for all couplings to cease. The reaction probability P^R is considered to be unity if the system smoothly transforms to products and the final s value is $\geqslant s_{\rm max}$. However, if there is a turning point for the relative translational motion before reaching the saddle point, it is necessary to evaluate a tunneling probability. Thus, for such trajectories, the reaction probability is approximated as the tunneling probability which is obtained using the WKB method:[33–37]

$$P_{\rm tunn}=\exp[-2I(s_1,s_2)] \tag{30}$$

where

$$I(s_1,s_2)=\frac{1}{\hbar}\int_{s_1}^{s_2} ds\left(\frac{2[H'_{\rm eff}(s)-E]}{1+2\epsilon(s,t)}\right)^{1/2}, \tag{31}$$

$$H'_{\rm eff}=V_0(s)+H_{\rm rot}+\hbar\sum_k\ \omega_k\left(\frac{1}{2}+\rho_k(t)\right), \tag{32}$$

and $\epsilon(s,t)$ contains coefficients of terms containing p_s^2 in Eq. (1):

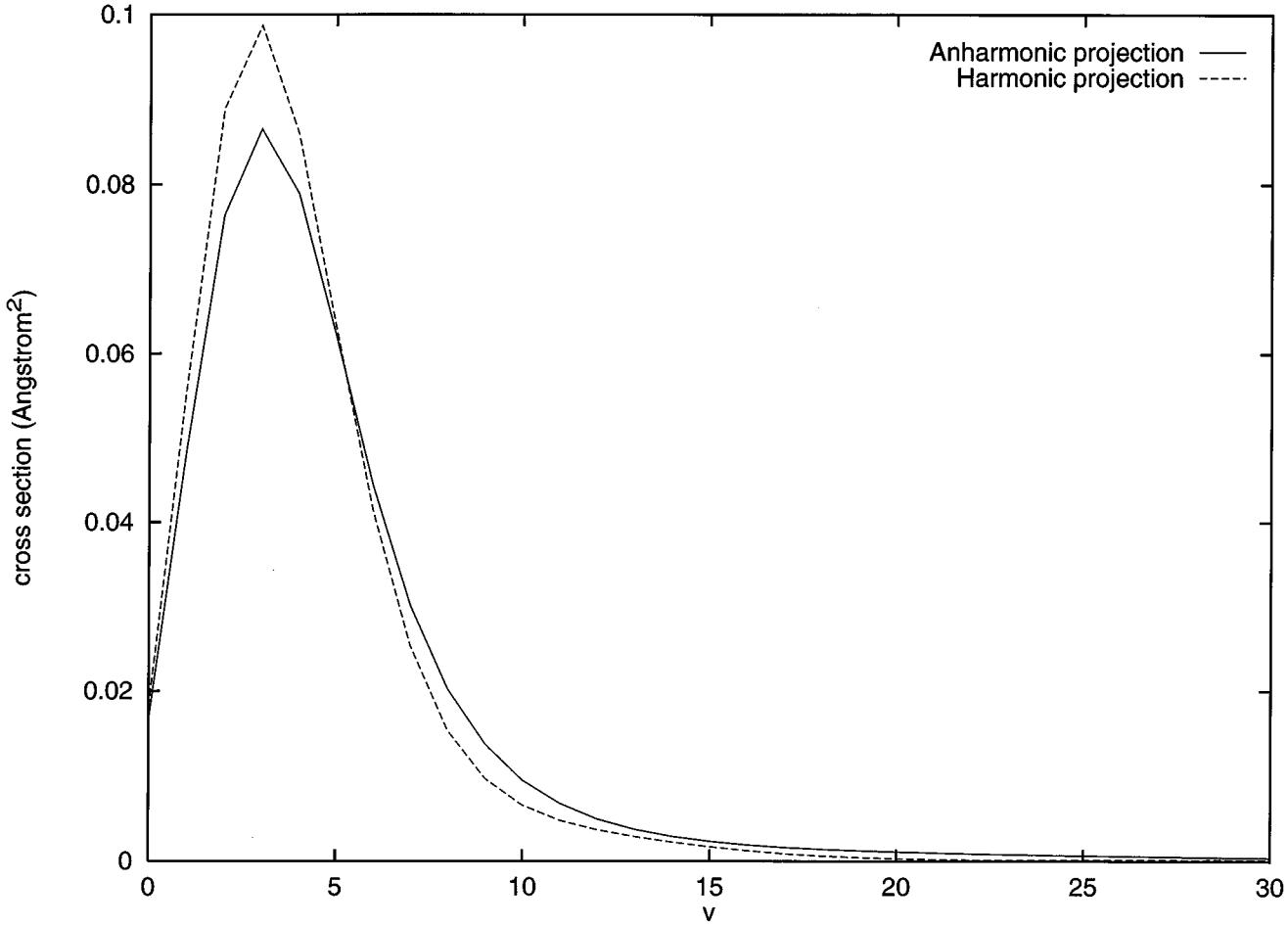

FIG. 5. Comparison of the vibrationally resolved cross section obtained by projecting the final wave function onto harmonic and anharmonic (exact) states of the diatomic fragments. The other O_2 molecule is taken to be in the ground vibrational state.

$$\epsilon(s,t)=\frac{\hbar}{2}\sum_k\left(\rho_k+\frac{1}{2}\right)\tilde{C}_{kk}/\omega_k(s)+i\sum_k\ (R_k^-P_k^+ - R_k^+P_k^-)+\frac{1}{2}\sum_{kl}\ \tilde{C}_{kl}b_kb_l\{(n_k^0Q_{kl}+n_l^0Q_{lk}^* + \alpha_l^+\alpha_k^-)+(n_k^0Q_{kl}^*+n_l^0Q_{lk}+\alpha_l^-\alpha_k^+)\}, \tag{33}$$

where

$$R_k^{\pm}=-B_{kF}(s)b_k(s)\exp(\pm i\theta_k). \tag{34}$$

The tunneling integral is evaluated at the classical turning point s_1 where $p_s\approx 0$. At s_1 E is set equal to $H_{\rm eff}$ and the trajectory is continued in the complex momentum space with $p_s\rightarrow ip_s$ until $E=H'_{\rm eff}(s_2)$. The dynamical variables except s are frozen between s_1 and s_2. At s_2, the integration is resumed in the real space with $p_s=0$ and $s=s_2$.

III. CROSS SECTIONS AND RATE CONSTANTS

The total reaction cross section is evaluated as[35]

$$\sigma=w_s\,\frac{\pi\hbar^2}{2\mu E_{\rm kin}(2j+1)}\sum_J\ (2J+1)P^R(E_{\rm kin},J), \tag{35}$$

where w_s is a statistical factor to account for more than one equivalent reaction paths. The initialization of the dynamics is performed as discussed in Sec. II A. If product state-resolved reaction probabilities are desired, one has to compute amplitudes of transitions to different product states which involves evaluating matrix elements of the V–V and V–T evolution operators at the end of the propagation. In this case, P^R should be replaced by P^R multiplied by the square of the transition amplitude given by Eq. (23). If the initial quantum states $\{n_i\}$ are all zero, then one only needs to solve the V–T problem as only elastic V–V transition is possible (V–V transitions include only those transitions where the vibrational quanta are conserved). Furthermore, in this case, the individual the V–T transition probabilities reduce to the familiar Poisson distribution as can easily be seen from Eq. (25).

Thermal rate constants are obtained by Boltzmann averaging the reaction probability over the initial rotational and translational energy distribution of the reagent molecule:[35,36]

$$k(T)=\sqrt{\frac{8k_BT}{\pi\mu}}\frac{\pi\hbar^2}{2\mu(k_BT)^2}\,\frac{w_s}{Q_{\rm rot}}\int_0^\infty dE_{\rm cl}\,\exp\left(-\frac{E_{\rm cl}}{k_BT}\right) \times J_{\max}2J(2J+1)P^R(E_{\rm cl},J), \tag{36}$$

where $Q_{\rm rot}$ is the rotational partition function for the reagent molecules, J is the total angular momentum and $J_{\rm max}$ is the maximum angular momentum of the complex at s_0:

$$J_{\rm max}=\frac{\sqrt{2E_{\rm cl}I^e_{xx}}}{\hbar}. \tag{37}$$

$E_{\rm cl}$ is the total classical energy which is the sum of rotational and kinetic energies and the moments of inertia $I^e_{xx}\approx I^e_{yy}\gg I^e_{zz}$. The total angular momentum $J=l+j$ where the orbital angular momentum l is chosen randomly between zero to $l_{\rm max}$ where $l_{\rm max}=\sqrt{(2\mu R(s_0)^2E_{\rm cl}}/\hbar$. The rotor angular momentum j is chosen randomly between $0-j_{\rm max}$ where $j_{\rm max}=\sqrt{2I(E_{\rm cl}-E_l)}/\hbar$ and I is given by Eq. (27). The orbital energy E_l is given by $E_l=\hbar^2l(l+1)/(2\mu R(s_0)^2)$. The projection quantum number K [see Eq. (26)] is chosen randomly between $-j$ to $+j$ and the total rotational energy is obtained as given by Eq. (26). The initial kinetic energy is then defined according to Eq. (28). Trajectories with $J>J_{\rm max}$ are rejected from the sampling space during the initialization.

IV. RESULTS AND DISCUSSION

Although reaction (R_1) is a very important process in the upper atmosphere, it is only rather recently that a reasonable PES for this reaction has become available. Varandas and Pais[16] have performed QCT calculations on their DMBE PES and reported total reaction cross section and thermal rate constants. Recently, Szichman *et al.*[17] have carried out approximate quantum mechanical calculations of this reaction on the DMBE surface and also reported total reaction cross section and thermal rate constants in good agreement with the QCT results. As mentioned in the introduction, we have[18] recently reported rate constants for reaction (R_1) using the VTST formalism. For the present calculation, altogether over a 1000 points have been computed along the reaction path from $s=-2.5$ to 5 amu$^{1/2}$ Å and the frequencies, moments of inertia, position vectors of different atoms and the orthogonal displacement vectors are spline fitted in a convenient form for use in the dynamics program. In Fig. 1, we have plotted the normal mode frequencies along the reaction path. As can be seen, asymptotically (in the O_3+O channel), the frequencies ω_3, ω_4, and ω_5 correlate with the bend, symmetric stretch and the antisymmetric stretch of the O_3 molecule. As one moves from $s=-\infty$ to $s=+\infty$, ω_4 and ω_5 becomes the vibrational frequencies of the two product O_2 molecules and ω_k, $k=1,3$ eventually correlate with the rotational and translational motions of the two molecules.

Since the coupling elements B_{kF}, $B_{kk'}$, and $\widetilde{C}_{kk'}$ are responsible for energy transfer to the perpendicular vibrational modes, it is possible to obtain important insight into the dynamics by examining some of these quantities as a function of s. For example, in Fig. 2, we have plotted the Coriolis coupling elements B_{kF} which couple the reaction path motion to the vibrational mode k for $k=3$, 4 and 5 as a function of s. It can be seen that in the product channel at $s\approx 3$ amu$^{1/2}$ Å the coupling element B_{4F} becomes large implying a large energy transfer to this mode. This is also evident from the sudden rise in frequency of this mode near the above s value as depicted in Fig. 1. The large increase in B_{4F} is also reflected in the frequency modulation term $\widetilde{C}_{44}$ illustrated in Fig. 3. The intermode coupling elements $\widetilde{C}_{45}$ is also appreciable at $s\approx 3$ amu$^{1/2}$ Å as seen in Fig. 3. The large increase in the coupling elements near the above s value is also reflected in the large increase in the internal energy of the system during the dynamics once it reaches this region. In particular, the vibrational mode 4 is preferentially excited with most of the internal energy being pumped into it. We have also monitored the quantity ρ_k during the dynamics which gives a measure of the vibrational excitation of the kth normal mode. This also shows that the O_2 molecule whose vibrational mode corresponds to mode 4 carries most of the internal energy. The other O_2 molecule is mostly formed in a low vibrational level.

The rotational excitation of the system during the reaction is found to be very little. This is partly due to the fact that the moments of inertia of the system do not change dramatically as one moves from the reactants to product valley as depicted in Fig. 4. Translational energy is found to be the most effective in promoting the reactivity as is typical for a reaction with an early barrier.

A. Reaction cross section

As mentioned in the introduction, it is possible to obtain final product vibrational state-resolved reaction cross sections or rate constants using the reaction path approach. The product vibrational state resolution is obtained by solving the V–T and V–V problem as discussed in Sec. II. Since the vibrational motions are treated within the harmonic approximation, the vibrational state resolution will be valid only for low vibrational states. As one of the O_2 molecules is produced in a relatively high vibrational state, it is desirable to project the final wave function onto different anharmonic states. Since the transition amplitude within the harmonic approximation is already obtained from the solutions of the V–T and V–V problem, the final wave function can be constructed using the harmonic oscillator wave function. One can then project this onto the different anharmonic (exact) states and obtain more accurate transition amplitudes. Since the diatomic part of the PES is composed of extended Rydberg wave functions, we have expanded the exact diatomic wave function in a basis of Morse oscillator wave functions. Fifty basis functions were found to be sufficient to represent the exact wave function for the $v=30$ state. The anharmonic transition amplitudes are obtained by projecting the final wave function onto the exact asymptotic wave functions thus constructed. Since the initial vibrational quantum numbers of the O_3 molecule are taken to be zero, only V–T transitions are possible. Thus, the final state distribution obtained within the harmonic approximation is the familiar Poisson distribution. In Fig. 5, we have compared the vibrational distribution of the O_2 molecule obtained from the harmonic and anharmonic projections. The difference between the two results are larger for higher v states though not clearly visible in the plot due to very small transition amplitudes. The vibrational state of the other molecule is taken to be the ground state.

The initial rotational energy of the O_3 molecules is taken

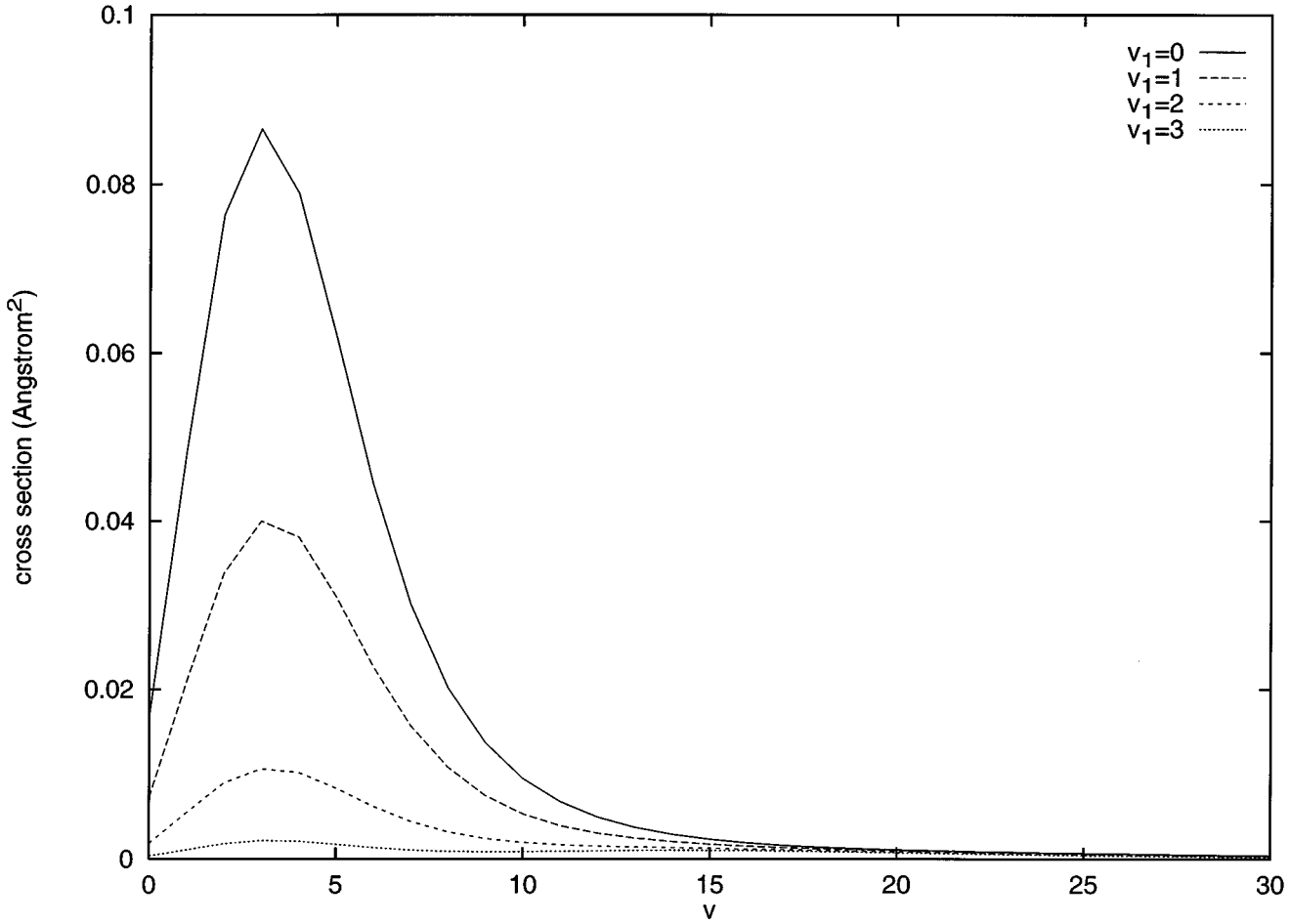

FIG. 6. Vibrational state-resolved cross sections obtained from the anharmonic projection as a function of the vibrational quantum number of one of the product O_2 molecules for different fixed vibrational states of the other. The cross sections are in Å^2 and the initial relative translational energy is 5 kcal/mol.

to be $3k_BT/2$ in order to facilitate the comparison of our results with those of Varandas and Pais[16] who used rotational energy along each principal axis to be $k_BT/2$. In our calculation for reaction cross section, we set $K=0$ in Eq. (26) and replaced I_1 by the average value given by Eq. (27) which results in $j\approx 27$ at $T=300$ K. (The principal moments of inertia of the O_3 molecule used in the calculation are $I_1=42.4$, $I_2=37.6$, and $I_3=4.7$ amu Å^2.) Thus, we have used $j=27$ and $K=0$ for the calculation of reaction cross section. The maximum impact parameter used is $b_{\max}=2.5$ Å below $E_{\rm kin}=0.25$ eV and $b_{\max}=3$ Å at higher energies. In Fig. 6, we have plotted the product state-resolved cross sections at $E_{\rm kin}=0.217$ eV (5 kcal/mol) as a function of vibrational state of one of the O_2 molecules for different fixed vibrational state of the other O_2 molecule. The results are averaged over 300 trajectories, and the error bars are typically 20%–25%. As can be seen, the distribution is broad, centered around $v=5$ but the tail extending beyond $v=25$. However, no bimodal pattern is seen in the distribution as was observed in the O_2 vibrational distribution obtained from O_3 photodissociation in recent experiments.[12,14]

In Fig. 7, we have presented similar vibrational state-resolved cross sections (summed over all final rotational states) at $E_{\rm kin}=0.26$ eV (6 kcal/mol) which also show a broad distribution of vibrational states. As discussed earlier, the large coupling at the exit of the product channel is responsible for the large vibrational energy transfer, and the O_2 molecule whose vibrational mode corresponds to the mode for which the coupling is highest is formed in the excited vibrational state. Since the vibrational distribution reduces to a poisson distribution within the harmonic approximation, the ρ_k values are a direct measure of the excitation of each mode. Since, to the best of our knowledge, there is no final state distribution of the product O_2 molecules reported in the literature, in Table I, we compare the results of our total reaction cross section (summed over all final rotational and vibrational states) with the QCT results of Varandas and Pais.[16] (read from Fig. 10 of Ref. 16). The QCT results increase more steeply with energy than the present results. Part of the discrepancy may be due to the difference in initialization of the dynamics and partitioning the initial rotational energy. The statistical factor w_s in Eq. (35) was assumed to be 2 while evaluating the cross sections. Furthermore, above barrier reflection also makes the reaction path results to become smaller at higher energies.

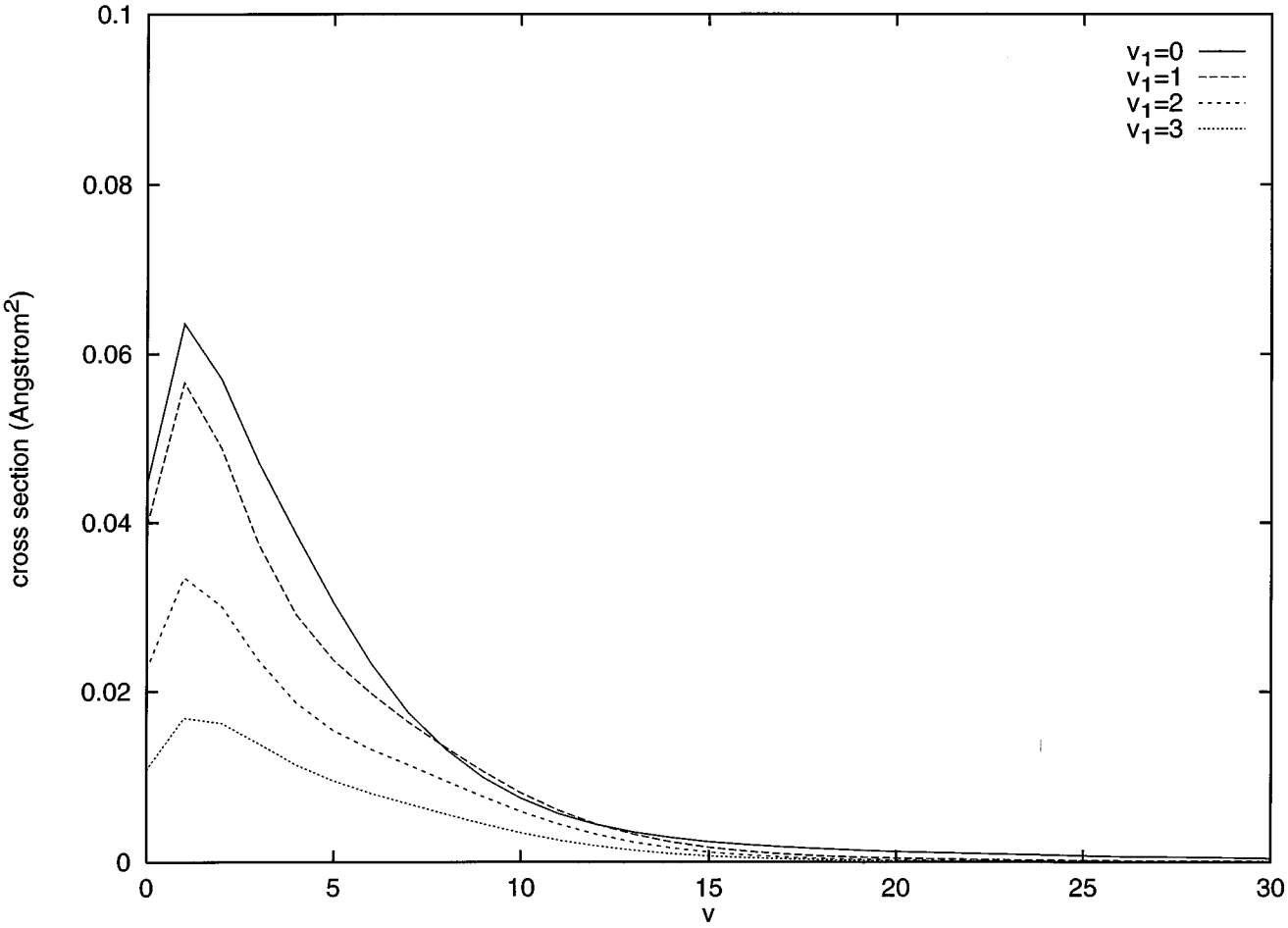

FIG. 7. Same as in Fig. 6, but for $E_{\rm kin}$=6 kcal/mol.

B. Thermal rate constants

Thermal rate constants are obtained by averaging the reaction cross section over the initial rotational and translational energies of the reagents as discussed in Sec. III. The O_3 molecule is initially assumed to be in the ground vibrational state. In Fig. 8, we have plotted the final state-resolved rate constants as a function of the vibrational state of the O_2 molecule formed in the excited vibrational state at three different temperatures: T=200, 300, and 400 K. The other molecule was taken to be in the ground vibrational state. As before, the statistical factor w_s was assumed to be 2 as the attacking O atom can approach any of the two terminal O atoms in O_3 with equal probability. We have also included an electronic degeneracy factor in the rate constants by multiplying the rate constants obtained from Eq. (36) with a factor $f_e(T)$ to approximately account for the degeneracies of the title reaction. $f_e(T)$ was taken to be the same as that suggested by Varandas and Pais:[16]

$$f_e(T)=\frac{3}{5+3\exp(-228/T)+\exp(-326/T)}, \tag{38}$$

which takes the limiting values 3/5 at T=0 and 1/3 at T =∞. For details regarding the choice of this function, see Ref. 15. As can be seen, the rate constant for the formation of O_2 in $v>25$ is quite small.

In Fig. 9, we compare the total thermalized rate constants obtained from the present calculations with the available theoretical results and different experimental results.[1,3,7] The theoretical results include the QCT results of Varandas and Pais,[16] the reduced dimensional quantum mechanical results of Szichman *et al.*,[17] and our recent VTST results.[18] As can be seen, reaction path results slightly underestimate the rate constants at higher temperatures. This has been observed in previous reaction path calculations[35,36] also and is probably due to the approximate harmonic treatment of the perpendicular vibrations which is believed to narrow the reaction valleys. Furthermore, since part of the energy is

TABLE I. Comparison of the total reaction cross section for reaction (R_1) from the present calculation and the QCT results of Varandas and Pais (Ref. 16).

E (kcal/mol)	σ (Å^2)	
	Present work	QCT
5	0.93	0.51± 0.08
6	1.16	0.84±14
7	1.2	1.3 ± 0.17

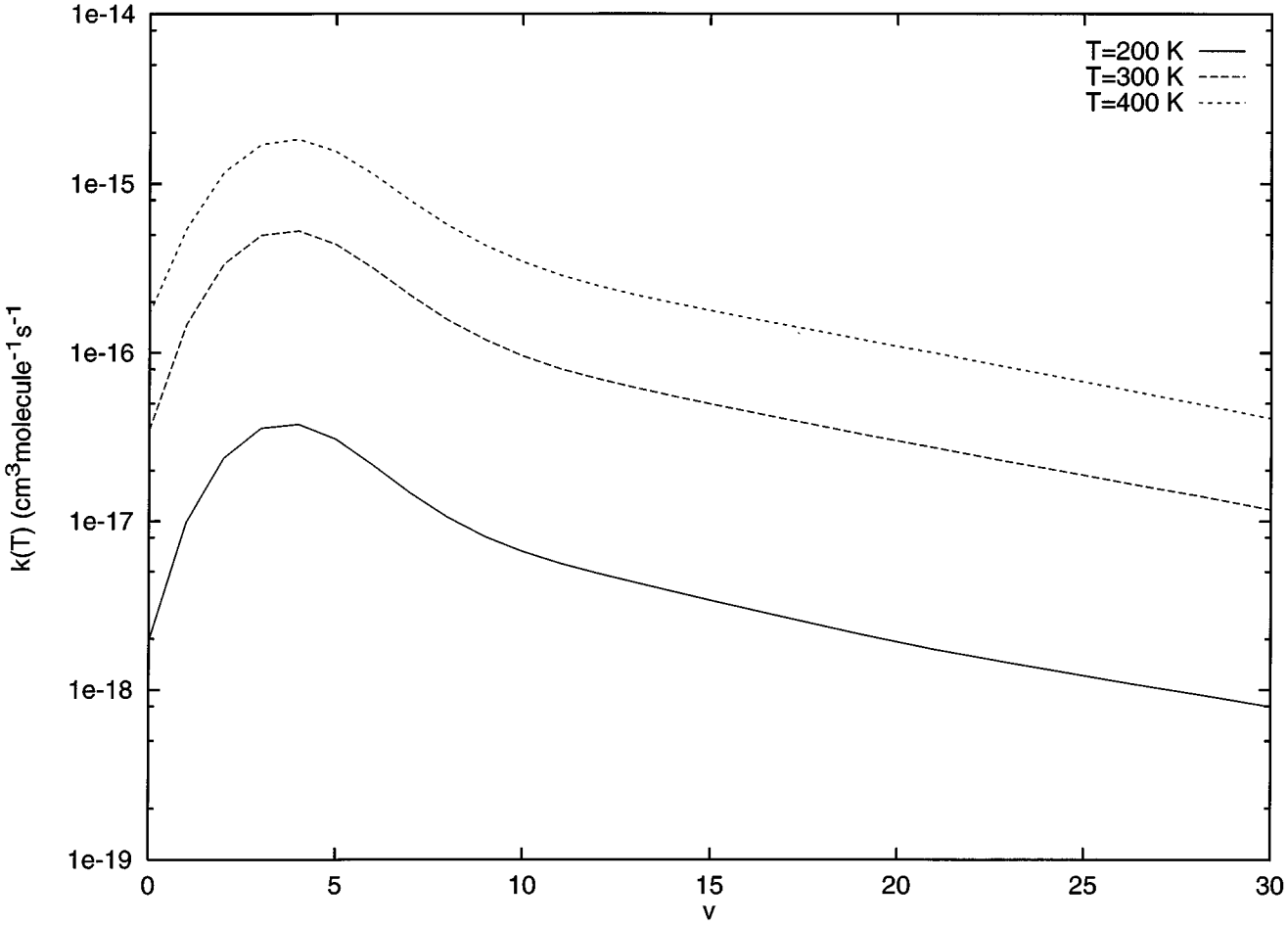

FIG. 8. Product vibrational state-resolved rate constants as a function of the vibrational quantum number of the O_2 molecule formed in the excited vibrational state. The results are for the ground vibrational state of the other O_2 molecule for three different temperatures: $T=200$, 300, and 400 K.

distributed among the rotational degrees of freedom, even at total energies higher than the barrier height, many trajectories get reflected, with a potential effect on reducing the reactivity. This is because, the rotational energy of the complex does not change appreciably during the dynamics and the rotational motion of the system essentially involves the overall rotation of the complex which does not cause reaction. Thus increasing the rotational energy of the complex has the effect of reducing the reactivity. It may be pointed out that the QCT rate constants are obtained by performing only a Boltzmann average over the initial translational energy of the system.

V. SUMMARY AND CONCLUSION

We have carried out a detailed investigation of reaction (R_1) using the reaction path formalism.[31–37] This approach, which treats the rotational and relative translational motions of the complex classically and the vibrational motions orthogonal to the reaction path quantally is able to give final product state-resolved reactive information. State-resolved cross sections and rate constants are important in modeling atmospheric reactions, in particular, if nonequilibrium situations exist which is the case when highly vibrationally excited species are involved. The present calculation clearly shows that one of the product O_2 molecules is formed in a relatively high vibrational state. This is in accord with the general observation for atom–diatom reactions in that the exothermicity goes mostly into product internal energy. Although the tail of the distribution extends to very high vibrational states, beyond $v=25$, the results are in general expected to be less accurate for very high v states because the dynamics is performed within the harmonic approximation, and only the final projection is carried out onto anharmonic states. But the harmonic basis set is still a complete basis in which the wave function can be expanded. If the harmonic coupling terms (treated to infinite order) are dominating then the simple harmonic/anharmonic projection technique will give reliable anharmonic probabilities and cross sections. As a matter of fact, it has recently been shown[39] that the simple anharmonic overlap model gives quite accurate results for energy transfer in proton–CF_4 collisions compared to those obtained from calculations with exact anharmonic couplings, if the molecule is initially taken in the ground vibrational state. However, it cannot at present be excluded that inclusion of anharmonic couplings will affect the final state dis-

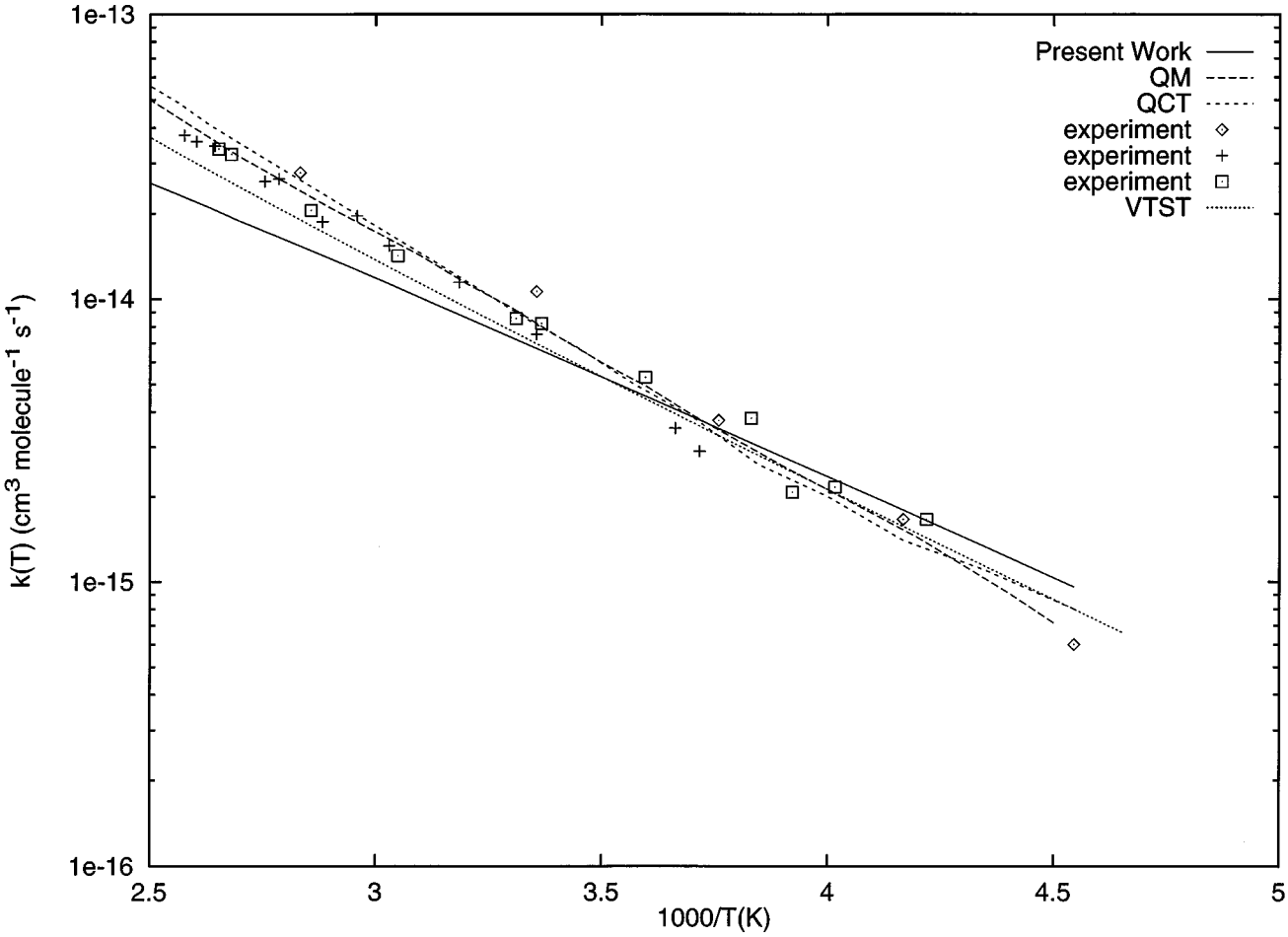

FIG. 9. Rate constants as a function of temperature for reaction (R_1): results of present calculation (solid line); QCT results from Ref. 16 (short-dashed line); QM results from Ref. 17 (long-dashed line); VTST results from Ref. 18 (dotted line); experimental results from Ref. 1 (+); experimental results from Ref. 3 (diamonds); experimental results from Ref. 7 (squares).

tribution and the reaction path approach is capable of including these coupling terms without any problems.

No bimodal pattern is seen in the O_2 vibrational distribution obtained from our calculation, in contrast to that observed for O_2 molecules produced from O_3 photodissociation. In principle, by utilizing the rate constants for (R_1) one could get an approximate estimation of the rate constants for reaction (R_2) by applying the microscopic reversibility. However, this is possible only if one has all relevant quantum numbers for the reagents as well as products. Since we obtain only product rotationally summed cross section, it is not possible to get a reliable estimate of the rate constant for the reverse process by the use of microscopic reversibility. In principle, it is possible to use the present approach to study reaction (R_2). In practice, describing the oscillator coordinates within the harmonic framework is highly unrealistic when vibrational states as high as $v=27$ is to be considered. However, preliminary results of our study[18] of reaction (R_2) using a semiclassical wave packet approach reported recently[19–21] was not indicative of any reaction within the limited number of trajectories propagated. Whether this has to do with the topography of the entrance channel (O_2+O_2) potential or the inadequacy of the dynamical scheme employed is not clear at this stage. It will be interesting to see if a direct measurement of the rate constants for reaction (R_2) is possible in the experimental studies.

ACKNOWLEDGMENTS

This research is supported by the Danish Natural Science Research Council and the Carlsberg Foundation.

[1] J. L. McCrumb and F. Kaufman, J. Chem. Phys. **57**, 1270 (1971).
[2] D. Husain, L. J. Kirsch, and R. J. Donovan, J. Photochem. **1**, 69 (1972).
[3] D. Davis, W. Wong, and J. Lephardt, Chem. Phys. Lett. **22**, 273 (1973).
[4] G. A. West, R. E. Weston, Jr., and G. W. Flynn, Chem. Phys. Lett. **56**, 429 (1978).
[5] S. K. Chekin, Y. M. Gershenzon, A. V. Konoplyov, and V. B. Rozenshtein, Chem. Phys. Lett. **168**, 386 (1979).
[6] I. Arnold and F. J. Comes, Chem. Phys. **42**, 231 (1979).
[7] P. H. Wine, J. M. Nicovich, R. J. Thompson, and A. R. Ravishankara, J. Phys. Chem. **87**, 3948 (1983).
[8] T. G. Slanger, L. E. Jusinski, G. Black, and G. E. Gadd, Science **241**, 945 (1988).
[9] H. Park and T. G. Slanger, J. Chem. Phys. **100**, 287 (1994).
[10] J. M. Price, J. A. Mack, C. A. Rogaski, and A. M. Wodtke, Chem. Phys. **175**, 83 (1993).
[11] X. Yang, J. M. Price, J. A. Mack, C. G. Morgan, C. A. Rogaski, D. McGuire, E. H. Kim, and A. M. Wodtke, J. Phys. Chem. **97**, 3944 (1993).

[12] R. L. Miller, A. G. Suits, P. L. Houston, R. Toumi, J. A. Mack, and A. M. Wodtke, Science **265**, 1831 (1994).
[13] D. Stranges, X. Yang, J. D. Chesko, and A. G. Suits, J. Chem. Phys. **102**, 6067 (1995).
[14] J. A. Sayage, J. Phys. Chem. **99**, 16530 (1995).
[15] P. J. Crutzen, J.-U. Grooβ, C. Brühl, R. Müller, and J. M. Russel III, Science **268**, 705 (1995).
[16] A. J. C. Varandas and A. A. C. C. Pais, in *Theoretical and Computational Models for Organic Chemistry*, edited by S. J. Formosinho, I. G. Czismadia, and L. G. Arnaut (Kluwer, Dordrecht, 1991), pp. 55–78.
[17] H. Szichman, A. J. C. Varandas, and M. Baer, J. Chem. Phys. **102**, 3474 (1995).
[18] N. Balakrishnan and G. D. Billing, Chem. Phys. Lett. **242**, 68 (1995).
[19] N. Balakrishnan and G. D. Billing, J. Chem. Phys. **101**, 2785 (1994).
[20] N. Balakrishnan and G. D. Billing, Chem. Phys. **189**, 499 (1994).
[21] N. Balakrishnan and G. D. Billing, Chem. Phys. Lett. **233**, 145 (1995).
[22] D. C. Clary, J. Chem. Phys. **95**, 7298 (1991); **96**, 3656 (1992).
[23] J. M. Bowman and D. Wang, J. Chem. Phys. **96**, 7852 (1992); D. Wang and J. M. Bowman, *ibid*. **98**, 6235 (1993).
[24] H. Szichman, I. Last, A. Baram, and M. Baer, J. Phys. Chem. **97**, 6436 (1993); H. Szichman and M. Baer, J. Chem. Phys. **101**, 2081 (1994).
[25] J. Echave and D. C. Clary, J. Chem. Phys. **100**, 402 (1994).
[26] D. H. Zhang and J. Z. H. Zhang, J. Chem. Phys. **99**, 5615 (1993); **100**, 2697 (1994).
[27] D. C. Clary, J. Phys. Chem. **98**, 10678 (1994).
[28] U. Manthe, T. Seideman, and W. H. Miller, J. Chem. Phys. **99**, 10078 (1993); **101**, 4759 (1994).
[29] D. H. Zhang and J. Z. H. Zhang, J. Chem. Phys. **101**, 1146 (1994).
[30] D. Neuhauser, J. Chem. Phys. **100**, 9272 (1994).
[31] G. D. Billing, Chem. Phys. **89**, 199 (1984).
[32] G. D. Billing, Comput. Phys. Rep. **1**, 237 (1984).
[33] G. D. Billing, Chem. Phys. **135**, 423 (1989).
[34] G. D. Billing, Chem. Phys. **146**, 63 (1990).
[35] G. D. Billing, Chem. Phys. **159**, 109 (1992).
[36] G. D. Billing, Chem. Phys. **161**, 245 (1992).
[37] G. D. Billing, N. Marković, and N. Balakrishnan, in *Dynamics of Molecules and Chemical Reaction*, edited by R. E. Wyatt and J. Zhang (Marcel Decker, New York) (to be published).
[38] G. D. Billing, Chem. Phys. **51**, 417 (1980).
[39] G. D. Billing, J. Chem. Soc. Faraday Trans. **86**, 1663 (1990).